HHS Public Access

Author manuscript

Nat Med. Author manuscript; available in PMC 2010 August 01.

Published in final edited form as:

Nat Med. 2010 February ; 16(2): 219–223. doi:10.1038/nm.2084.

Neutrophil Elastase-Mediated Degradation of IRS-1 Accelerates Lung Tumor Growth

A. McGarry Houghton[1,4,5], **Danuta M. Rzymkiewicz**[6], **Hongbin Ji**[7], **Alyssa D. Gregory**[1,4], **Eduardo E. Egea**[1,4], **Heather E. Metz**[1,4], **Donna B. Stolz**[2,5], **Stephanie R. Land**[3,5], **Luiz A. Marconcini**[6], **Corrine R. Kliment**[1], **Kimberly M. Jenkins**[1,4], **Keith A. Beaulieu**[1,4], **Majd Mouded**[1,4], **Stuart J. Frank**[8], **Kwok K. Wong**[9], and **Steven D. Shapiro**[1,4,5]

[1]Department of Medicine, University of Pittsburgh School of Medicine, Pittsburgh, PA 15213

[2]Department of Cell Biology & Physiology, University of Pittsburgh School of Medicine, Pittsburgh, PA 15213

[3]Department of Biostatistics, University of Pittsburgh School of Medicine, Pittsburgh, PA 15213

[4]Division of Pulmonary, Allergy, and Critical Care Medicine, University of Pittsburgh School of Medicine, Pittsburgh, PA 15213

[5]University of Pittsburgh Cancer Institute, University of Pittsburgh School of Medicine, Pittsburgh, PA 15213

[6]Division of Pulmonary and Critical Care Medicine, Brigham and Women's Hospital, Boston, MA 02115

[7]Institute of Biochemistry & Cell Biology, Shanghai Institute for Biological Sciences & Chinese Academy for Sciences, Shanghai, China

[8]Division of Endocrinology, Diabetes, and Metabolism, University of Alabama at Birmingham, Birmingham, AL 35294.

[9]Ludwig Center at Dana-Farber/Harvard Cancer Center, Departments of Medicine and Medical Oncology, Dana-Farber Cancer Institute & Harvard Medical School, Boston, MA 02115.

Summary

Lung cancer is the leading cause of cancer death worldwide1. Recent data suggest that tumor-associated inflammatory cells may modify lung tumor growth and invasiveness2-3. To determine the role of neutrophil elastase (NE or *Elane*) on tumor progression, we utilized the *LSL-K-ras* model of murine lung adenocarcinoma4 to generate *LSL-K-ras/Elane*$^{-/-}$ mice. Tumor burden was markedly reduced in *LSL-K-ras/Elane*$^{-/-}$ mice at all time points following induction of mutant K-ras expression. Kaplan-Meier life survival analysis demonstrated that while 100% of *LSL-K-ras/*

Address correspondence to A.M.H. (houghtonm@dom.pitt.edu).

Author Contributions. A.M.H. and S.D.S. designed this study and interpreted all data. A.M.H., D.M.R., H.J., A.D.G., E.E.E, H.E.M., D.B.S., L.A.M., C.R.K., K.M.J., K.A.B., and M.M. performed the experiments. S.R.L. performed statistical analyses. S.J.R. provided the IRS1 expression vector and assisted with data interpretation. K.K.W. participated in study design and data interpretation. A.M.H. wrote the manuscript.

Elane$^{+/+}$ mice died, none of the mice lacking NE died. NE directly induced tumor cell proliferation in both human and mouse lung adenocarcinomas by gaining access to an endosomal compartment within tumor cells where it degraded insulin receptor substrate-1 (IRS1). Co-immunoprecipitation studies showed that as NE degraded IRS1, there was increased interaction between PI3K and the potent mitogen platelet derived growth factor receptor (PDGFR) thereby skewing the PI3K axis toward tumor cell proliferation. The inverse relationship identified between NE and IRS1 in *LSL-K-ras* mice was also identified in human lung adenocarcinomas, thus translating these findings to human disease. This study identifies IRS1 as a key regulator of PI3K within malignant cells. Additionally, this is the first description of a secreted proteinase gaining access to a cell beyond its plasma membrane and altering intracellular signaling.

Lung cancer is the leading cause of cancer related deaths worldwide with dismal ~15% five-year survival rates despite therapeutic advances over the preceding decades1. A better understanding of tumor-associated inflammation may identify novel therapeutic targets.

Neutrophils are known to infiltrate tumors, however, only recently have they been thought to modify tumor growth and invasiveness2-7. We have previously shown that lung cancer cells elaborate CXC chemokines driving neutrophil recruitment. Hence, tumor-associated neutrophils don't necessarily represent a means of host defense. Indeed, there have been reports that neutrophil infiltrates within tumors correlate with poor clinical outcomes9-10.

The purpose of this study was to determine if the most potent neutrophil proteinase, NE, played a role in tumor progression. NE is a neutrophil-specific serine proteinase with broad substrate specificity. Its expression is limited to promyelocyte stages of bone marrow development where it is packaged into azurophil granules11. The main function of NE is to eliminate pathogens within neutrophils12-13. However, upon activation, neutrophils translocate NE to the cell surface and secrete small amounts of enzyme from individual granules14.

We subjected Lox—Stop—Lox K-ras^{G12D}/Elane$^{-/-}$ (*LSL-K-ras/Elane*$^{-/-}$) and control (*LSL-K-ras/Elane*$^{+/+}$) mice to 5×10^6 pfu intratracheal adenoviral cre recombinase (AdenoCre) to activate mutant K-ras expression4. During the 28 weeks following AdenoCre administration, all *LSL-K-ras/Elane*$^{+/+}$ but none of the *LSL-K-ras/Elane*$^{-/-}$ mice died. Survival analysis demonstrated a significant (P=0.006) advantage for *LSL-K-ras/Elane*$^{-/-}$ mice (Fig. 1a). NE-deficiency is not completely protective, as we have subsequently identified death beyond 30 weeks in independent studies. Tumor burden was markedly reduced in *LSL-K-ras/Elane*$^{-/-}$ mice at all time points (Fig. 1b,d–f). The differences observed represent a reduction in tumor growth and differentiation (less mature lesions), as tumor number was equivalent in the two groups (Supplementary Table 1). NE-mediated effects on tumor growth are not model specific, as similar reductions in tumor growth were observed in the Lewis Lung carcinoma model using WT and *Elane*$^{-/-}$ mice (Supplementary Fig. 1).

Immunohistochemical (IHC) analyses and lung lavage cell counts demonstrated equivalent neutrophil content and distribution in *LSL-K-ras/Elane*$^{-/-}$ and *LSL-K-ras/Elane*$^{+/+}$ mice (Fig. 1c,g), thereby excluding a role for NE in neutrophil trafficking. We also excluded the

unlikely possibility that *LSL-K-ras* tumors produced NE using casein zymography (not shown).

We identified significant reductions in tumor cell proliferation in *LSL-K-ras/Elane*$^{-/-}$ mice (Fig. 1h,i) using Ki-67 IHC. Immunofluorescence (IF) staining demonstrated differential activity in the PI3K pathway (pAkt), but specifically not in MEK/ERK (Fig. 1j). Proteinases can release growth factors sequestered within extracellular matrix for use by tumors14-15, which could account for these findings. However, we were unable to detect differences between the groups for relevant growth factors (not shown).

We examined the possibility that NE could directly induce tumor cell proliferation and performed co-culture experiments utilizing WT and *Elane*$^{-/-}$ PMN to demonstrate an essential requirement for NE in PMN-mediated tumor cell proliferation (Fig. 2a). Neutrophils only release ~2% of their NE content upon activation resulting in modest concentrations (~50 nM) just beyond the cell surface16. Dose response curves in *LSL-K-ras* tumor-derived cell lines (Fig. 2b) confirmed that modest concentrations of NE (40-80 nM) induced cellular proliferation, while excessive concentrations caused cell death (Fig. 2b). We reproduced NE-induced proliferation in two human lung adenocarcinoma cell lines, A549 (K-ras mutant) and 201T (K-ras WT)(Fig. 2c–e). The effects of NE required catalytic activity, as inactive NE (heated or synthetic inhibitor) failed to induce proliferation (Supplementary Fig. 2).

Dependence of NE-induced proliferation upon PI3K was demonstrated using an inhibitor (LY294002), whereas inhibition of the MEK/ERK pathway (U0126) had no effect (Fig. 2f). NE exposure induced pAkt (Fig. 2g), as expected for a PI3K dependent process. Phospho-p44/42-MAPK production was not affected (Fig. 2h).

Alexa488-labeled NE was utilized to identify the site of NE and tumor cell interaction. Surprisingly, NE gained access to tumor cells beyond their plasma membrane. The enzyme was localized to early endosomal antigen-1^{+} (EEA1) endosomes (but not calveolae) (Fig. 2i), known to shuttle cargo from clathrin pits to other cellular locations17. Endosomal NE was required for cell proliferation, as inhibition of endosome formation (using dynasore18) prevented proliferation (Fig. 2j).

Of growth factors known to activate PI3K, the PDGF/PDGFR complex is an attractive candidate to drive tumor cell proliferation. It's a potent inducer of pAkt via PI3K, is not found in lung epithelial cells, but is highly expressed in non-small cell lung cancer (NSCLC)19. Both the ligand and the receptor are produced in NSCLC thereby creating a potent autocrine loop for PI3K activation. *LSL-K-ras* tumors also express PDGF and PDGFR (Fig. 3a).

Treating A549 cells with NE at cell-proliferative concentrations didn't alter the quantity of PDGF, PDGFR, or p-PDGFR (Fig. 3b). NE-exposure did increase interaction (co-immunoprecipitation) between the p85 subunit of PI3K and PDGFR (Fig. 3c,d). Gene silencing confirmed dependence of NE-induced proliferation on PDGFR (Fig. 3e,f).

The PI3K axis is uniquely regulated within each cell type20. We reasoned that NE must degrade a homeostatic binding partner of p85. Loss of such a binding partner would create an opportunity for PDGF/PDGFR to recruit and activate p85. We identified a number of potential NE-substrates within the PI3K pathway, including IRS1, an adaptor protein known to bind p8521. In fact, IRS1 and PDGF have been shown to differentially regulate PI3K activity in adipocytes, generating opposing effects on cell behavior despite activating the same p85 subunit22.

NE rapidly hydrolyzed IRS1 at 1:100 molar concentrations (Fig. 4a). Cell proliferative concentrations of NE eliminated IRS1 within A549 cells (Fig. 4b). Silencing of *IRS1* gene expression induced tumor cell proliferation (Fig. 4c). Marked IRS1 over-expression reduced tumor cell growth and abrogated the proliferative effects of NE, confirming that IRS1 loss is a required event in this process (Fig. 4d). Hence, independent of NE, IRS1 is capable of regulating tumor cell proliferation.

IRS1 isn't located on the cell surface nor sequestered in the ECM. Therefore, NE: IRS1 interaction must occur within the cell, a distinct possibility given the trafficking studies presented in Fig. 2i. Confocal microscopy of NE-exposed A549 cells co-localized NE and IRS1 within tumor cells (Fig. 4e). Remarkably, Irs1 protein was significantly reduced in *LSL-K-ras/Elane*$^{+/+}$ compared to *LSL-K-ras/Elane*$^{-/-}$ tumors *in vivo* (Fig. 4f,g). However, *Irs1* mRNA levels were equivalent between the two groups by qPCR (Fig. 4h), consistent with degradation of the protein.

IRS1 has been reported to function in both pro-tumor and pro-host capacities23. The phosphorylation status of IRS1 may dictate behavior, with pTyr IRS1 functioning as a positive effector of growth factor and pSer producing a regulatory factor24. IRS1 accumulation in *LSL-K-ras/Elane*$^{-/-}$ tumors was predominantly serine-phosphorylated (Fig. 4i), consistent with this hypothesis.

Han *et al*. reported that IRS1 staining was absent in 43.6% of Stage I NSCLC, correlating with increased tumor size25. We performed NE and IRS1 IHC on 38 human lung adenocarcinomas to confirm an inverse relationship between NE and IRS1 (Fig. 4j). We used likelihood ratio tests to demonstrate that the proportion of discordant views (NE and IRS1 were considered discordant when either one was present but the other was absent/faint in the same view) was statistically significant ($P<0.001$).

These results may partially explain PI3K hyperactivity in NSCLC despite infrequent mutation in PTEN, the constitutive negative repressor of PI3K20. Our findings suggest that IRS1 is a key regulator of PI3K. We propose that the downstream consequences of p85 binding by IRS1 are fundamentally different (more homeostatic) than those for potent growth factors such as PDGFR. If IRS1 levels were depleted (NE-mediated degradation), or its ability to bind p85 altered (G972R polymorphism26), increased cancer susceptibility may result. In fact, G972R confers increased prostate cancer risk27. Aberrant autocrine loops (PDGF—PDGFR) would be required to significantly skew the net function of PI3K. Consistent with this hypothesis, NE didn't induce proliferation in lung epithelial cells (PDGFR^{-}) but did in fibroblasts (PDGFR^{+}) (Supplementary Fig. 3).

NE exists within neutrophil azurophil granules for rapid transit to phagolysosomes where it kills bacteria during acute infection12-13. If “dumped” into ECM, NE causes tissue destruction. In the lung, unopposed NE degrades elastin resulting in emphysema28. NE may also cause cell death at high concentrations, but these concentrations are not likely achievable in vivo. At physiologic concentrations, NE was actively transported to a sub-cellular location and increased cell proliferation. The ability of a secreted proteinase to enter another cell and alter cell signaling represents a new concept in proteinase biology, and expands the list of both potential substrates and functions for proteinases.

Small molecule inhibitors of NE have been developed for, although never adequately tested in, COPD. To demonstrate the plausibility of NE-inhibition as cancer therapy, we treated *LSL-K-ras* mice with the NE inhibitor, ONO-5046, or vehicle, for 14 weeks post-AdenoCre. Administration of the inhibitor reduced lung tumor growth by three-fold ($P<0.05$) (Supplementary Fig. 4). The results presented here might spur enthusiasm to test these agents in NSCLC, especially in light of the recent finding that emphysema predisposes to the development of lung cancer29-30. NE may explain the link between the two diseases. As neutrophils and NE are recruited to the lungs of smokers to promote emphysema, sub-clinical nodules would become more aggressive. Hence, NE inhibition might be an attractive approach to treat both diseases, which currently account for ~300,000 deaths per year in the U.S. alone.

Methods

Mice

Neutrophil elastase deficient mice (*Elane*$^{-/-}$) on a C57BL6 background have been described elsewhere28. Lox-Stop-Lox K-ras^{G12D} (*LSL-K-ras*) mice provided by Tyler Jacks have been described elsewhere4 and have subsequently been backcrossed into C57BL6 > five generations. Induction of mutant K-ras expression and the use of ONO-5046 is described in Supplementary Methods. All experiments described herein were approved by the Harvard Standing Committee for Animal Welfare or the University of Pittsburgh IACUC committee.

Tissue processing

The lungs were inflated with 10% buffered formalin at 25 cm H2O pressure via an intratracheal catheter for 10 min. The lungs were removed and fixed in 10% buffered formalin for 24 hr before embedding in paraffin.

Histology and Immunohistochemistry

Serial mid-sagittal 5 μm sections were used for H&E staining and IHC. Tumor burden was reported as the percentage of lung area occupied by tumor (tumor area μm^2/total area μm^2) on 50 different 10X sections per slide. IHC was performed as described4 using antibodies against PDGF (Upstate), PDGFRα/β (Upstate), IRS1 (Abcam) and Ki-67 (DAKO). The proliferative index was reported as the number of Ki-67 positive cells per tumor area. Lung tissue immunofluorescence was performed on frozen sections for phospho proteins not amenable to detection on routinely fixed tissues. Detailed methods are located in the Supplementary Methods.

Human lung adenocarcinoma cases (FFPE) obtained from the Lung SPORE tissue bank were subjected to NE and IRS1 IHC (Abcam). These studies were deemed “exempt” by the University of Pittsburgh Institutional Review Board. Four fields identified on the NE slide were imaged, and then the corresponding field in the IRS1 slide was imaged. Images were scored: NE, absent=0, present=2, 1-2 cells=1; and IRS1, absent=0, faint=1, present=2, heavy=3. NE=1 slides were excluded from the analysis. NE and IRS1 were considered discordant when whether one was present but the other absent/faint in the same view. For each tumor sample, the number of discordant views was modeled with a binomial distribution. Likelihood ratio tests determined whether the proportion of discordant views was significantly greater than one-half, the proportion that would be expected by chance.

Cells

The human lung adenocarcinoma cell line A549 (K-ras mutant) was used for in vitro experiments (ATCC). Key experiments were duplicated in K-ras WT 201T lung adenocarcinoma cells (ATCC), and murine lung adenocarcinoma cell lines derived from *LSL-K-ras* tumors as previously described8. All cells were maintained in DMEM plus 10% FCS, 1X NEAA, and 1X penicillin/streptomycin.

Thymidine incorporation

Cells were plated at a concentration of 1×10^5 cells/well in 24-well plates before treatment with NE at concentrations from 4—400 nM (Elastin Products) for 60 min in serum-free media, washing with PBS, and incubation in serum-free media containing 1 μCi/mL of thymidine (Perkin Elmer) for an additional 18 hrs. Assays were terminated by washing with PBS, fixing with 5% TCA, and washing with H_2O. Cells were then dissolved in 300 mL 200 mM NaOH neutralized with equimolar HCl and transferred to scintillation vials. LY294002 (1.0 μM)(Upstate), U0126 (10 μM)(Cell Signaling), PMSF (1 mM)(Sigma) and dynasore32 (40 μM)(Sigma) were utilized in a subset of experiments. DMSO was the control vehicle for the LY294002, U0126, and dynasore experiments. Results from representative experiments in triplicate. All experiments were replicated at least three times.

Confocal microscopy was employed to determine the location of NE within tumor cells and to identify interaction with other proteins. Detailed procedures are located in the Supplementary Methods.

Western blotting

Standard 10% SDS-PAGE was performed followed by transfer of proteins to a nitrocellulose membrane. The following antibodies and dilutions were used: pAkt (1:250, Cell Signaling), Akt (1:500, Cell Signaling), p85 (1:500, Upstate), IRS-1 (1:500, Upstate), IRS-2 (1:500, Upstate), PDGF (1:250, Upstate), PDGFRα (1:250, Upstate), pPDGFRα (1:250, Upstate), p44/42-MAPK (1:500, Cell Signaling), phospho-p44/42-MAPK (1:500, Cell Signaling), and pEGFR (1:250, Cell Signaling). β-actin (1:1000, Cell Signaling) served as the endogenous control. All experiments performed in triplicate. All experiments were replicated at least three times.

Co-immunoprecipitation

Lysates from NE-treated A549 cells and controls were immunoprecipitated with anti-p85 or anti-pTyr-p85 antibodies (Upstate) immobilized to protein A/G agarose resin according to manufacturer's instructions (Pierce). Following elution, the samples were subjected to Western blot using anti-PDGFRα (Upstate). All experiments performed in triplicate. All experiments were replicated at least twice.

Protein expression

IRS-1 protein was over-expressed in A549 cells using a lipofectamine transfection of pcDLSRα containing WT IRS135. Lipofectamine only transfection served as control. Western blotting confirmed IRS1 expression.

siRNA

A549 cells were plated in 24-well plates at 5×10^4 cells/well. PDGFRα (Invitrogen), IRS-1 (Dharmacon), or SCR siRNA (Invitrogen) (all 40 nM), were transfected using Lipofectamine per manufacturer's instructions (Invitrogen). Cells were washed with PBS 6 hrs later. Western blot analyses and thymidine incorporation assays were performed two days later. All assays were performed in triplicate and replicated at least three times in separate experiments.

Statistics

Data are expressed as the mean value ± SEM. Simple pair-wise comparisons were analyzed using the student's t-test (two tailed distribution with two sample equal variance). For multiple comparisons, one-way ANOVA with Newman-Keuls post-test was employed. A *P* value of <0.05 was considered significant. The Kaplan-Meier survival curve analysis employed a log-rank test.

Supplementary Material

Refer to Web version on PubMed Central for supplementary material.

Acknowledgements

This work was supported by grants K08HL085286 and RO1HL054853 from the NIH/NHLBI (A.M.H. and S.D.S.) and by grant RO1DK058259 from the NIH/NIDDK (S.J.F). ONO Pharmaceutical (Osaka, Japan) provided the ONO-5046. AdenoCre was obtained from the University of Iowa Gene Transfer Vector Core. The authors would like to recognize members of the Shapiro lab for their assistance and comments regarding the preparation of this manuscript.

Abbreviations

NE	Neutrophil Elastase
IRS-1	Insulin receptor substrate-1
PDGF	Platelet derived growth factor
PDGFR	PDGF-receptor

PI3K	Phosphtidylinositol-3 kinase
A1AT	Alpha-1 antitrypsin
MMP	Matrix metalloproteinase
AdenoCre	Adenoviral cre recombinase

References

1. Jemal A, et al. Cancer statistics 2009. CA Cancer J. Clin. 2009; 59:225–249. [PubMed: 19474385]
2. Karin M. Inflammation and cancer: the long reach of Ras. Nat. Med. 2005; 11:20–21. [PubMed: 15635437]
3. Coussens LM, Werb Z. Inflammation and cancer. Nature. 2002; 420:860–867. [PubMed: 12490959]
4. Jackson EL, et al. Analysis of lung tumor initiation and progression using conditional expression of oncogenic K-ras. Genes Dev. 2001; 15:3243–3248. [PubMed: 11751630]
5. Sparmann A, Bar-Sagi D. Ras-induced interleukin-8 expression plays a critical role in tumor growth and angiogenesis. Cancer Cell. 2004; 6:447–458. [PubMed: 15542429]
6. Haqqani AS, Sandhu JK, Birnboim HC. Expression of interleukin-8 promotes neutrophil infiltration and genetic instability in mutatect tumors. Neoplasia. 2000; 2:561–568. [PubMed: 11228549]
7. Nozawa H, Chiu C, Hanahan D. Infiltrating neutrophils mediate the initial angiogenic switch in a mouse model of multistage carcinogenesis. Proc. Natl. Acad. Sci. 2006; 103:12493–12498. [PubMed: 16891410]
8. Ji H, et al. K-ras activation generates an inflammatory response in lung tumors. Oncogene. 2006; 25:2105–2112. [PubMed: 16288213]
9. Bellocq A, et al. Neutrophil alveolitis in bronchioloalveolar carcinoma. Am. J. Pathol. 1998; 152:83–92. [PubMed: 9422526]
10. Foekens JA, et al. The prognostic value of PMN leukocyte elastase in patients with primary breast cancer. Cancer Res. 2003; 63:337–341. [PubMed: 12543785]
11. Lee WL, Downey GP. Leukocyte Elastase: Physiological functions and role in acute lung injury. Am. J. Respir. Crit. Care Med. 2001; 164:896–904. [PubMed: 11549552]
12. Belaaouaj A, et al. Mice lacking neutrophil elastase reveal impaired host defense against gram-negative bacterial sepsis. Nat. Med. 1998; 4:615–618. [PubMed: 9585238]
13. Weinrauch Y, Drujan D, Shapiro SD, Weiss J, Zychlinsky A. Neutrophil elastase targets virulence factors of enterobacteria. Nature. 2002; 417:91–94. [PubMed: 12018205]
14. Lee S, Jilan SM, Nikolova GV, Carpizo D, Iruela-Arispe ML. Processing of VEGF-A by matrix metalloproteinases regulates bioavailability and vascular patterning in tumors. J. Cell. Biol. 2005; 169:681–691. [PubMed: 15911882]
15. Wada Y, et al. Neutrophil elastase induces cell proliferation and migration by the release of TGFα, PDGF and VEGF in esophageal cell lines. Oncology Reports. 2007; 17:161–167. [PubMed: 17143494]
16. Liou TG, Campbell EJ. Quantum proteolysis resulting from release of single granules by human neutrophils: a novel, nonoxidative mechanism of extracellular proteolytic activity. J. Immunol. 1996; 157:2624–2631. [PubMed: 8805666]
17. Rubino M, et al. Selective membrane recruitment of EEA1 suggests a role in directional transport of clathrin-coated vesicles to early endosomes. J. Biol. Chem. 2000; 275:3745–3748. [PubMed: 10660521]
18. Antoniades HN, et al. Malignant epithelial cells in primary human lung carcinomas coexpress in vivo platelet-derived growth factor (PDGF) and PDGF receptor mRNAs and their protein products. Proc. Natl. Acad. Sci. 1992; 89:3942–3946. [PubMed: 1315044]
19. Macia E, et al. Dynasore, a cell-permeable inhibitor of dynamin. Developmental Cell. 2006; 10:839–850. [PubMed: 16740485]

20. Cully M, You H, Levine A, Mak TW. Beyond PTEN mutations: the PI3K pathway as an integrator of multiple inputs during tumorigenesis. Nat. Rev. Cancer. 2006; 6:184–192. [PubMed: 16453012]
21. Yamauchi T, et al. Growth hormone and prolactin stimulate tyrosine phosphorylation of insulin receptor substrate-1, -2, and –3, their association with p85 phosphatidylinositol 3-kinase (PI3-kinase), and concomitantly PI3-kinase activation via JAK2 kinase. J. Biol. Chem. 1998; 273:15719–15726. [PubMed: 9624169]
22. Nave BT, Haigh RJ, Hayward AC, Siddle K, Shepherd PR. Compartment-specific regulation of phosphoinositide 3-kinase by platelet-derived growth factor and insulin in 3T3-L1 adipocytes. Biochem. J. 1996; 318:55–60. [PubMed: 8761452]
23. Dearth RK, Cui X, Kim H-J, Hadsell DL, Lee AV. Oncogenic transformation by the signaling adaptor proteins insulin receptor substrate (IRS)-1 and IRS-2. Cell Cycle. 2007; 6:705–713. [PubMed: 17374994]
24. Gual P, Le Marchand-Brustel Y, Tanti JF. Positive and negative regulation of insulin signaling through IRS-1 phosphorylation. Biochimie. 2005; 87:99–109. [PubMed: 15733744]
25. Han CH, et al. Clinical significance of insulin receptor substrate-1 down-regulation in non-small cell lung cancer. Oncology Reports. 2006; 16:1205–1210. [PubMed: 17089038]
26. Sentinelli F, et al. The G972R variant of the insulin receptor substrate-1 gene impairs insulin signaling and cell differentiation in 3T3L1 adipocytes; treatment with a PPARγ agonist restores cell signaling and differentiation. J. Endocrinol. 2006; 188:271–285. [PubMed: 16461553]
27. Neuhausen SL, et al. Prostate cancer risk and IRS1, IRS2, IGF1, and INS polymorphisms: strong association of IRS1 G972R variant and cancer risk. Prostate. 2005; 64:168–174. [PubMed: 15678496]
28. Shapiro SD, et al. Neutrophil elastase contributes to cigarette smoke-induced emphysema in mice. Am. J. Pathol. 2003; 163:2329–2335. [PubMed: 14633606]
29. Wilson DO, et al. Association of radiographic emphysema and airflow obstruction with lung cancer. Am. J. Resp. Crit. Care Med. 2008; 178:738–44. [PubMed: 18565949]
30. Houghton AM, Mouded M, Shapiro SD. Common origins of lung cancer and COPD. Nat. Med. 2008; 10:1023–1024. [PubMed: 18841139]

Reference for Methods

31. Rice WR, et al. Maintenance of the mouse type II cell phenotype in vitro. Am. J. Physiol. 2002; 283:L256–64.
32. Kliment CR, et al. Oxidative stress alters syndecan-1 distribution in lungs with pulmonary fibrosis. J Biol Chem. 2009; 284:407–10.
33. Yasuoka H, et al. Insulin-like growth factor-binding protein-5 induces pulmonary fibrosis and triggers mononuclear cellular infiltration. Am. J. Pathol. 2006; 169:1633–42. [PubMed: 17071587]
34. Houghton AM, et al. Macrophage elastase (MMP-12) suppresses the growth of lung metastases. Cancer Res. 2006; 66:6149–6155. [PubMed: 16778188]
35. Tu Y, Liang L, Frank SJ, Wu C. Src homology 3 domain-dependent interaction of Nck-2 with insulin receptor substrate-1. Biochem J. 2001; 354:315–322. [PubMed: 11171109]

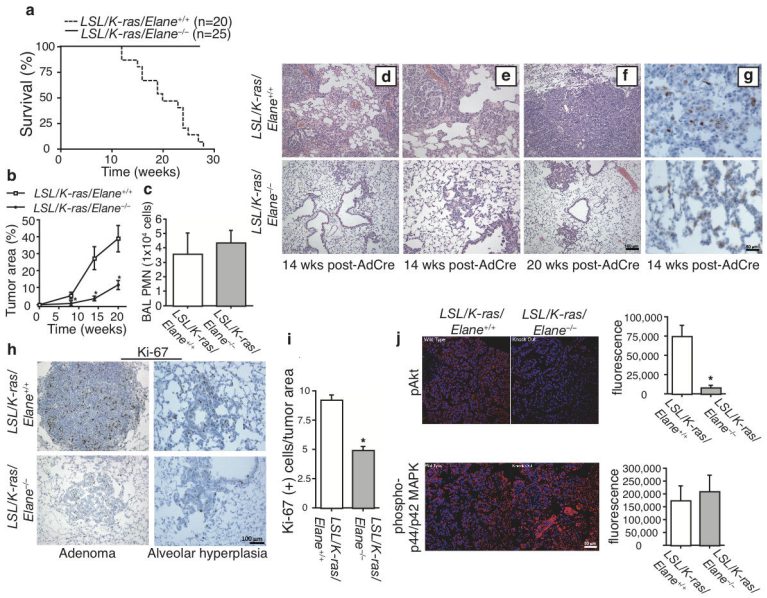

Figure 1. NE promotes lung tumor growth in vivo

(a) Kaplan-Meier Survival curve for AdenoCre recipient *LSL/K-ras/Elane*$^{+/+}$ and *LSL/K-ras/Elane*$^{-/-}$ mice; *P*=0.006, log-rank test. **(b)** Tumor area (%) for both groups at 8, 14, and 20 weeks post-AdenoCre. N=5 mice per group. Bars ± SEM. **P*<0.01. **(c)** BALF neutrophil counts for AdenoCre recipient *LSL/K-ras/Elane*$^{+/+}$ and *LSL/K-ras/Elane*$^{-/-}$ mice at the 14-week time point. N=5 mice per group. Bars ± SEM. *P*=NS. Representative H&E images at 14 weeks **(d, e)** and 20 weeks **(f)** post-AdenoCre. **(g)** Representative images for anti-p40^{phox} (anti-neutrophil) IHC at 14 weeks post-AdenoCre. (**h**) Representative Ki-67 IHC 14 weeks post-AdenoCre. **(i)** Ki-67 (+) cells per tumor area for N=5 mice per group at the 14-week time point. Bars ± SEM. **P*<0.01. **(j)** Representative IF images and quantification for pAkt and phospho-MEK/ERK from both groups of mice 14 weeks post-AdenoCre. Bars ± SEM. *P*<0.01 for pAkt.

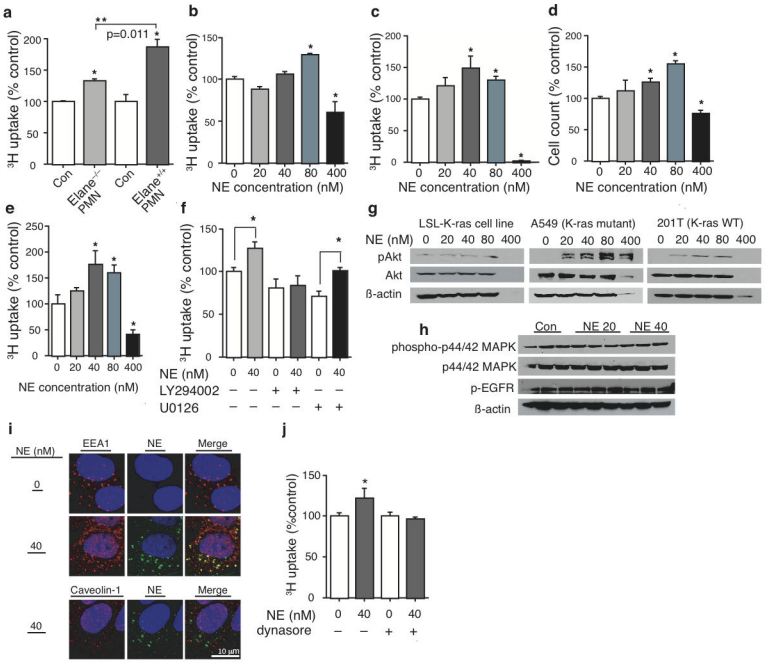

Figure 2. Neutrophil Elastase induces tumor cell proliferation

(a) ^{3}H uptake for *LSL-K-ras* tumor-derived cell lines5 co-incubated with WT and *Elane*$^{-/-}$ PMN for two hours. Results from a representative experiment in triplicate. Bars ± SEM. **P*<0.05 from control. ***P*=0.011, ANOVA. **(b)** ^{3}H uptake for *LSL-K-ras* cells stimulated with NE or vehicle for 60 min. Data from a representative experiment in triplicate. Bars ± SEM. **P*<0.01 from NE=0. **(c)** ^{3}H uptake and **(d)** cell counts for A549 cells and ^{3}H uptake for **(e)** 201T cells (K-ras WT). Results from representative experiments in triplicate. Bars ± SEM, *P*<0.05 from NE=0. **(f)** ^{3}H uptake for A549 cells stimulated with NE in presence or absence of 1.0 μM LY294002 or 10 μM U0126 for 60 min. Results from a representative experiment in triplicate. Bars +/− SEM. *P*<0.05. (g) Western blots of pAkt, Akt and B-actin for NE-exposed lysates of A549, 201T, and *LSL-K-ras* cells. **(h)** Western blot of phospho-p44/42-MAPK, p44-42-MAPK, pEGFR, and B-actin for NE-exposed A549 lysates. **(i)** Confocal images for EEA1, caveolin-1, and NE from A549 cells exposed to AlexaFluor488-conjugated NE or vehicle. Nuclei were counterstained using DAPI. **(j)** ^{3}H uptake for A549 cells stimulated with NE ± 40 μM dynasore. Results from a representative experiment in triplicate. Bars +/− SEM. **P*<0.05.

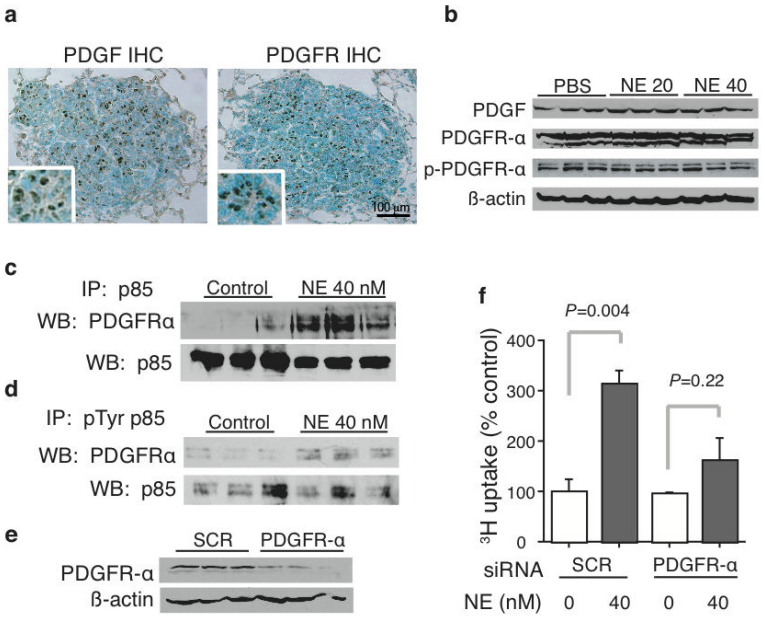

Figure 3. NE-induced proliferation is dependent upon PDGFR—PI3K signaling

(a) Representative images for PDGF and PDGFR IHC of *LSL/K-ras* tumors. *Inset*, high magnification showing PDGF and PDGFR staining within cells displaying tumor morphology. **(b)** Western blots for PDGF, PDGFRα, pPDGFRα and β-actin from NE-exposed A549 cell lysates. Results from a representative experiment in triplicate. Immunoprecipitation of **(c)** p85 and **(d)** phospho-tyrosine p85 from A549 cell lysates followed by Western blotting for PDGFRα. Membranes stripped and probed for p85. **(e)** Representative blot for PDGFRα following siRNA treatment with SCR siRNA vs. PDGFRα siRNA. **(f)** ^{3}H uptake for PDGFRα-silenced A549 cells subsequently exposed to NE or vehicle. Results from a representative experiment in triplicate. Bars +/− SEM. **P*<0.001.

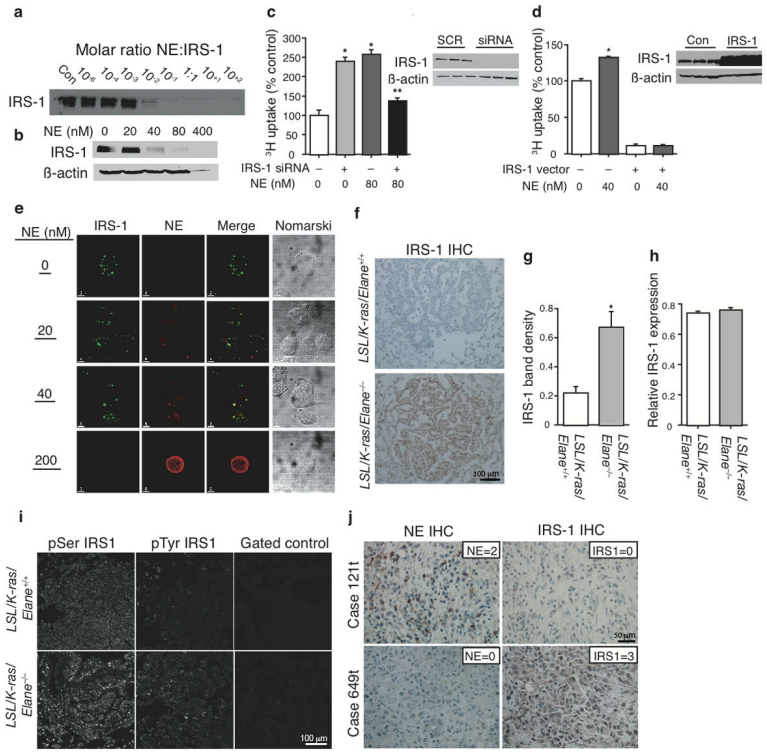

Figure 4. NE co-localizes with and degrades IRS-1

(a) IRS-1 Western blot following incubation of recombinant IRS-1 protein with NE over a range of molar ratios. **(b)** IRS-1 and β-actin Western blots for NE-exposed A549 cell lysates. **(c)** ^{3}H uptake for IRS-1 silenced (or SCR control) A549 cells subsequently exposed to NE or vehicle. Results from a representative experiment in triplicate. Bars ± SEM. **P*<0.001 from NE=0 control. ***P*<0.05 from NE=80. *Inset*, IRS-1 blot of SCR and IRS-1 siRNA treated lysates. **(d)** ^{3}H uptake for IRS-1 over-expressing A549 cells subsequently exposed to NE or vehicle. Results from a representative experiment in triplicate. Bars ± SEM. **P*<0.01. *Inset*, IRS-1 blot of IRS-1 vector and control treated lysates. **(e)** Confocal images for IRS-1 and NE from A549 cells exposed to NE (or vehicle). **(f)** Representative IRS-1 IHC images from *LSL/K-ras/Elane*$^{+/+}$ and *LSL/K-ras/Elane*$^{-/-}$ mice 14 weeks post-AdenoCre. **(g)** IRS-1 Western blot for 14-week post-AdenoCre tumor homogenates from both groups (N=5). Results presented as relative band density ± SEM. *P*<0.001. (**h**) IRS-1 real-time PCR for 14-week post-AdenoCre tumor homogenates from both groups (N=4). Results expressed as GAPDH CT/IRS-1 CT ± SEM. **(i)** Representative IF images for pSer and pTyr IRS-1 from *LSL/K-ras/Elane*$^{+/+}$ and *LSL/K-ras/Elane*$^{-/-}$ tumors 14-wks post-AdenoCre. **(j)** Representative images of human lung adenocarcinoma specimens for NE=2 and IRS-1=0 (Case 121t) and NE=0 and IRS-1=3 (Case 649t). NE and IRS-1 were considered discordant when either one was present but the other absent/faint in the same view. The empirical probability of discordance was 0.88, which was significantly greater than chance (0.5), *P*<0.001.